Pump probe imaging of nanosecond laser induced bubbles in agar gel

R. Evans and S. Camacho-Lopez

Centro de Investigacion Cientifico y Educacion Superior de Ensenada, Baja California, Mxico, 22860

F. Perez and G. Aguilar

UC Riverside, Irbine CA, 90210

revans@cicese.mx

Abstract: In this paper we show preliminary results of of our pump-probe laser machining stage used on 1mm thick agar gels to study Nd:YAG laser induced bubbles formed by a 9ns, 532nm laser pulse tightly focused inside the bulk of the gel sample. With our system we measured the the bubble formation and shock wave speed with nanosecond and micrometer resolution. The shock waves generated by the laser are shown to begin at an eariler time during the laser pulse as the pulse energy increases. The bubble created reaches a quasi-stable size that has a linear relation to the maximum bubble size. The energy stored in the bubble is also shown to increase nonlinearly with applied laser energy. We think that these last two facts point to the role that laser produced plasma has in the production of the bubble.

OCIS codes: (000.0000) General.

References and links

1. A. Brujan and A. Vogel, "Stress wave emission and cavitation bubble dynamics by nanosecond optical breakdown in a tissue phantom," J. Fluid Mech. **558,** 281-308 (2006).
2. K. R. Rau and P. A. Quinto-Su and A. N. Hellman and V. Venugopalan, "Pulsed Laser microbeam-induced cell lysis: Time-resolved imaging and analysis of hydrodynamic effects," Biophysical Journal **91,**317-329(2006).
3. C. B. Schaffer and N. Nishimura and E. Glezer and A. M. T. Kim and E. Mazur, "Dynamics of femtosecond laser-induced breakdown in water from femtoseconds to microseconds," Optics Express **3,10**196-204(2002).
4. A. Vogel and V. Venugopalan, "Mechanisms of pulsed laser ablation of biological tissues," Chemical Reviews **103, 2**577-644, 2003).

1. Introduction

The use of lasers in biological applications has been growing steadly as the technology becomes more stable and aforadable. While the laser is not necessarily an efficient method to delivery energy, it is one of the most precise, and can allow for the greatest finesse. The studies that we present here are aimed at the control of laser tissue ablation and measuring the secondary effects caused by the use of short pulse lasers; mainly the strong shock waves that are the precursor to the eventual bubble expansion.

We use agar gel because it presents a simple tissue phantom. The melting point of agar gel is very close to the boiling point of water, and the point of cellular damage in animal tissue. It has been well documented that a nanosecond laser focused inside of liquids and gels will cause

the formation of a bubble[1, 2] These studies have also presented an analysis of the growth and collapse of the bubble. The study presented here adds to the litature by giving nanosecond time resolution, allowing for a percise measure of the bubble growth, collapse, and associated shock wave. The high numerical aperture used (0.5) allows for a much lower pulse energy then was used others such as Vogel, minimizing heating of the gel before the beam is focused, and also keeping the energy to a reasonably low value; which should be used for eye and skin surgery.

The bubble continues to grow long after the laser pulse has finished, which implies that the initial conditions that the laser sets, completly defines (along with the material parameters) the life of the bubble. Several papers have shown, with picosecond resolution [3] , the beginning of bubble formation but only in liquids and solids, and with the longest times scanned being on the order of nanoseconds. Work done at long time scales are forced to rely on simulations and assumptions for the beggining hundred nanoseconds [1, 4]. With our system we can fill in this hole; Rau also had nanosecond to millisecond time scales, but their delay was made with fiber delay lines which limited the maximum delay.

This article will present the experimental setup, the preliminary results and finally a brief discussion to both interperate the observations and place them into current litature.

2. Experimental System

2.1. Laser sources

Our optical system consisted of two frequency doubled (make**) Q-switched Nd:YAG lasers. One of the two lasers had a half-wave plate polarizer pair to control the power onto the doubling crystal; the laser had been modified to permit the rejected IR beam from the polarizer to escape. We used the green 532nm beam from the unmodified laser as our pump beam, and the IR 1064nm beam as the probe. Agar gel has a flat absorption spectrum from 500 to 1400 nm with an absorption less then 10%. The CCD used for imaging the sample has a higher quantum efficiency for IR light (after removing its IR filter) so the IR beam was chosen as the probe beam and the green as the pump. The IR probe beam typically had less then 1microJoul of energy per pulse which allowed for an OD=1 neutral density filter to be placed in front of the CCD to remove stray light.

The two beams were brought onto the sample co-linear. The green pump beam was roughly collimated before it fell onto the 6mm (NA=0.5) aspherical machining lens; the pump beam, which over-filled the lens, was reduced in size by a diaphram placed before the lens. The IR probe beam was focused by a 35cm lens to a point before the machinig lens such that it was collimated as it propagated through the sample. After the sample we used a 25mm lens and 40cm lens to image relay the IR beam onto a CCD placed in the transmitted beam line. The image relay was focused for the IR beam, and the green pump was removed with a red colour filter.

The 35mm lens in the IR beam line also served a second purpose. The CCD could be placed to have the pump beam retro-reflected from the target (usually the surfaces of the glass slides in the agar target) onto the CCD in another image relay; this setup is commonly refereed to as an equivalent target plane (ETP.) The ETP was used to set the location of the beam focus in the sample when each new sample was placed. The pump beam energy was monitored with a cross-calibrated energy monitor placed on the green reflection of the IR input beam splitter (the calibration was done with a second energy monitor **(make) placed after the machining lens.) The IR probe beam was filtered out before the energy monitor. The per pulse energy was acquired by the monitor display, then imported and stored in a computer. The energies measured were exact and not averages.

The pump laser used had a $1/e^2$ pulse duration of 9.2ns and was focused to a beam waist $1/e^2$ radius of $2.3\mu m$; measured with the ETP system. The probe laser passed the sample with

a spot size of $350\mu m$ with a per pulse energy close to $1\mu J$.

2.2. *Timing*

The timing of the pump to probe delays was controlled with a Stanford DG535 delay generator. The DG535 was triggered by the flash output of the CCD camera which was triggered by either the computer or a hand-held button. The DG535 sent triggers to the flash lamp and Q-switch inputs of both lasers. The pump-probe zero time delay was set with a photodiode placed after the sample holder and read on an oscilloscope. The DG535 allowed for delays up to nine seconds with picosecond time resolution. The CCD camera had a shutter time of typically 400ms, and was set to open about 10ms before the arrival of the pump pulse.

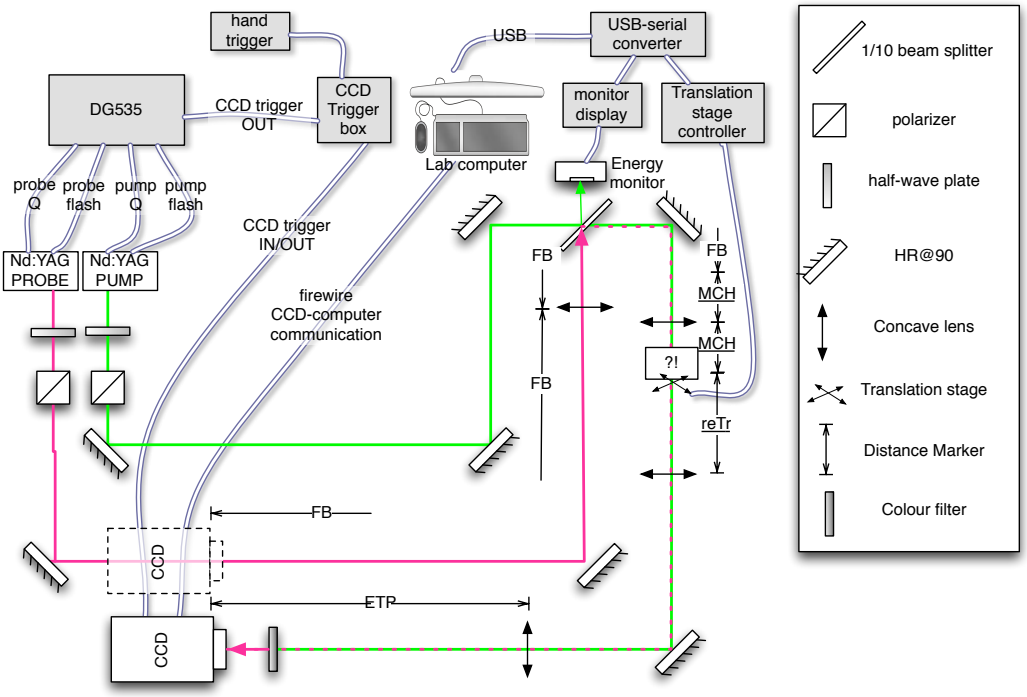

Fig. 1. Optical system. Two Nd:YAG lasers, one of which is frequency doubled, are shone on target with a delay controlled by a DG535. The 535nm pump beam is focused on target while the 1064nm beam passes the target colliminated. The two locations of the CCD are used to image the sample in transmission and reflection. The system can be triggered by a hand-held trigger or through the computer; both of which control the CCD which then sends a trigger to the DG535.

2.3. *Target alignment and preparation*

The image relay systems above was used in conjunction with a three axis (x,y,z) computer controlled translation stages; one micron step size. The samples of agar were mixed with a concentration of 1g agar powder per 50mL of distilled water. Once heated to melting point in a double boiler (to avoid burning) the agar was pored between two microscope slides separated by 1mm spacers. The sample was left to cool before placement onto its gimbled target holder in the machining system. The target holder allowed for adjustment of the surface to beam angle

from which we attained a vertical change of less then $50\mu m$ over a horizontal slide of 4cm. This allowed us to set the beam focus to the center of the 1mm thick sample and to take hundreds of data points quickly (less then 20min) with no overlap and or loss of focus location.

3. Results

The laser was focused in the center of the 1mm agar sample. One pulse was exposed per site. The time delays were set to observe three distinct regions of interest;

- 0 to 100ns with $\Delta t = 20ns$: Shock wave propagation speed
- 200ns to $1\mu s$ with $\Delta t = 200ns$: Bubble maximum size
- $1\mu s$ to $100\mu s$ with $\Delta t = 3\mu s$: Bubble collapse
- $100\mu s$ to 1ms with $\Delta t = 30\mu s$: Far field bubble size

Other time delays such as those used in Fig. 2 were used to probe a variety of times. Shown in figure 2 are the results in a log-log plot for several typical energies of the bubble size vs. time; in the example image shown in the insert of Fig. 2 both the bubble formation and shock wave are visable. The field of view of the CCD camera and size of the probe beam allowed for a maximum bubble size that could be measured to be about $450\mu m$ in diameter.

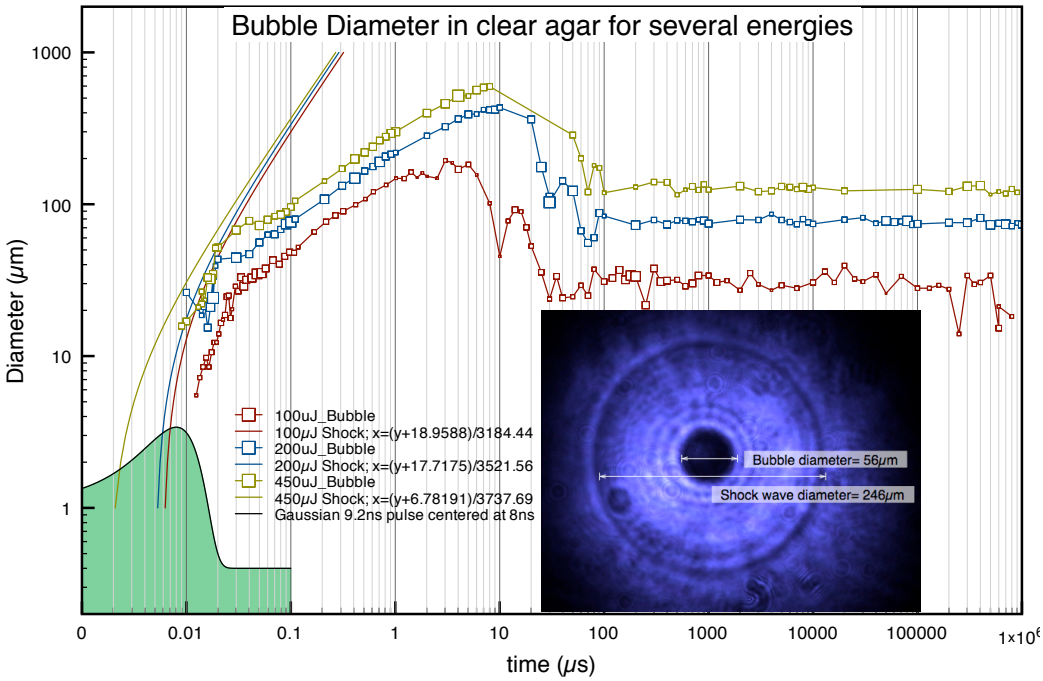

Fig. 2. Log-log plot of the formation of a bubble. The shock wave diameters are from fits to the measured points; the points are not on the plot to reduce cluttering. The laser pulse drawn is found from a fit to the pulse location as discussed below and shown in Fig. 6. Picture insert; image captured by CCD camera for an agar sample taken 60ns after the arrival of a $250\mu J$ laser pulse. The bubble and shock wave diameters are noted.

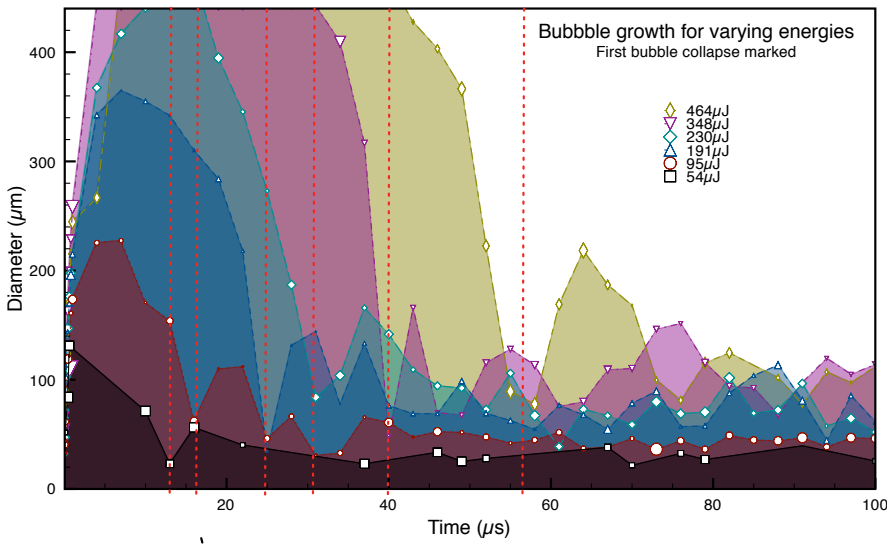

Fig. 3. Time variation of bubble formed by laser pulses of varying energy. The time till the first collapse of the bubble is noted by a red dotted line.

The bubble diameter varied less then 10% from $100\mu s$ to hundreds of seconds. We dubbed the bubble size at 1ms the farfield bubble size. This size has a near linear relation to the maximum bubble size, Fig.4. It should be noted that the bubble does not always collapse to the same center location, and was seen many times to collapse to one side, but its edge did not extend further then the edge of the maximum bubble, and the bubble always retained its proportional size.

An advantage of of the system used here is the ability to measure the location of the shock wave. The shock wave velocity is directly related to the pressure difference between the illuminated region and its surrounding region **ref**. By measuring this velocity we can then deduce the initial conditions of the bubble, instead of using complicated simulations and assumptions such as those needed by other authors [4] . By linear fitting the shock wave diameter we found the shock wave velocity and the x-intercept, the latter of which is related to the time of launch of the shock as shown in Fig. 5.

Rau [2] has shown evidence that bubble formation is linked to plasma formation in the focal volume of the laser pulse. If this is true, there will exist a light irradiance fluence above which plasma will form. Plasma has a much higher absorption of laser light then the low absorption agar, so the sooner that threshold is reached, the proportionally more laser energy the region will absorb. As well, laser energy is coupled into the electrons in a plasma and from there into the positive ions; this happens on the order of picoseconds. This means that the expansion of the hot medium will happen in a time shorter then our 9ns laser pulse.

Considering the beginning of the shock waves to have a direct relation to the time in the laser pulse when the threshold irradiance is reached we then looked for this relation to x-intercpt of the shock wave and laser pulse energy. The laser pulse is well represented by a gaussian profile:

$$I(t) = I_0 exp\left[\frac{-2(t-t_0)^2}{\tau^2}\right] \tag{1}$$

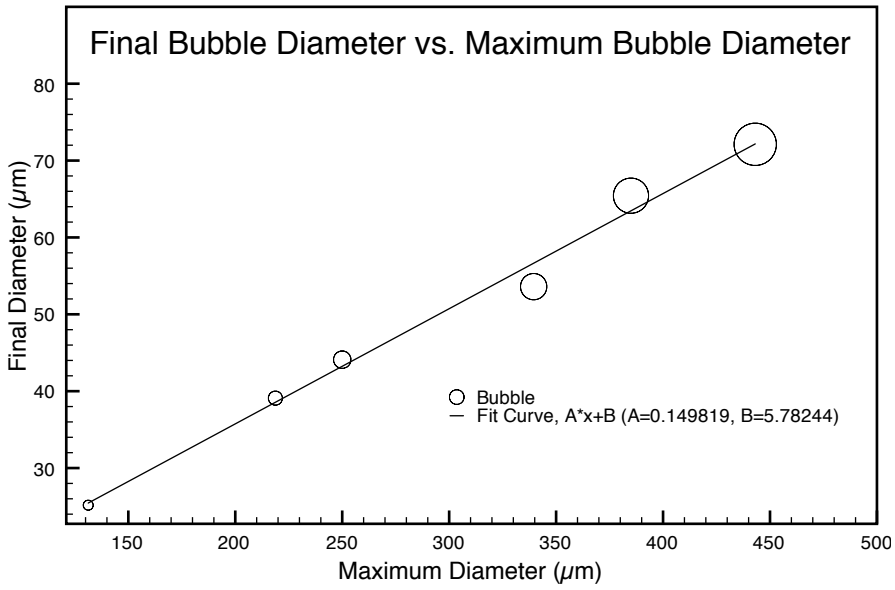

Fig. 4. A linear dependance of the bubble size at 1ms to it's maxium size. The size of the data point is proportional to the per pulse laser energy.

Equation 1 can be solved for t_n; the time at which a laser pulse with peak irradiance, I_n, reaches the threshold irradiance for plasma formation; $I_n(t_n) = I_{threshold}$ to give:

$$t_n = \frac{\tau}{2}\sqrt{Log\frac{I_{threshold}}{I_n}} - t_0 \tag{2}$$

Recall the relation between irradiance to energy in a pulse $\frac{I_{th}}{I_n} = \frac{E_{th}}{E_n}$ where E_{th} is the energy in a pulse whose peak irradiance is I_{th}, which gives;

$$t_n = \frac{\tau}{2}\sqrt{Log\frac{E_{th}}{E_n}} - t_0 \tag{3}$$

Equation 3 was then used as a fit function to the x-intercept found in Fig. 5 to solve for the location of the pulse center time t_0 and the pulse threshold energy E_{th}; shown in Fig. 6. For our experiments this gave a pulse center time of 8ns and a threshold energy of $76\mu J$. In our experiments we found the threshold to be on the order of $55\mu J$.

Of interest as well is the energy that the laser transfers to the medium. Again we use Rau's [2] example as a reference. There they use the case explored by Lord Rayleigh for an interially controlled bubble growth. From there the energy in the bubble can be expressed as a function of the maxium radius and the time of the first collapse of the bubble;

$$E_B = \frac{2}{3}\pi\rho\left(\frac{0.915}{T_{col}}\right)^2 R_{max}^5 \tag{4}$$

Where E_B is the energy in the bubble, T_{col} is the time till the first collapse, and R_{max} is the maximum bubble radius. In Fig. 7 the ratio of the energy in the bubble to the energy in the laser pulse is shown. The energy in the bubble reaches close to 0.5% of the laser pulse power, and

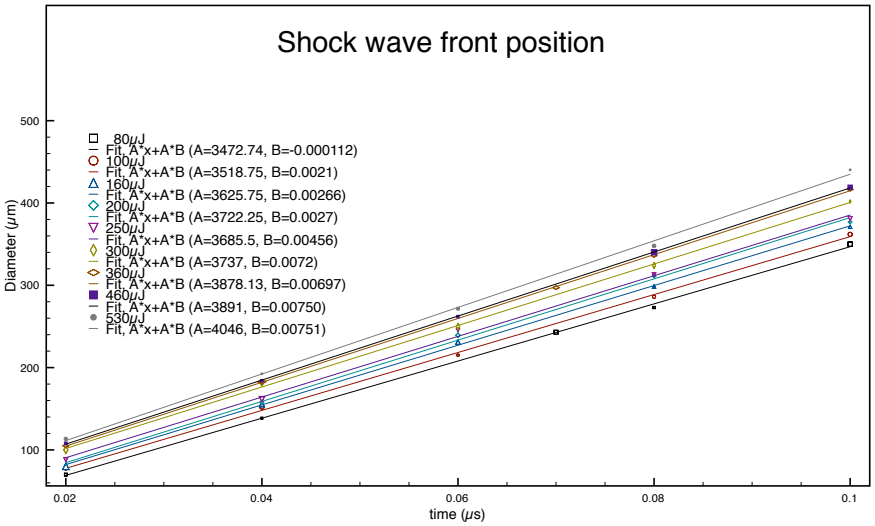

Fig. 5. The shock wave front for varying energies gives the shock wave velocity and the x-intercept.

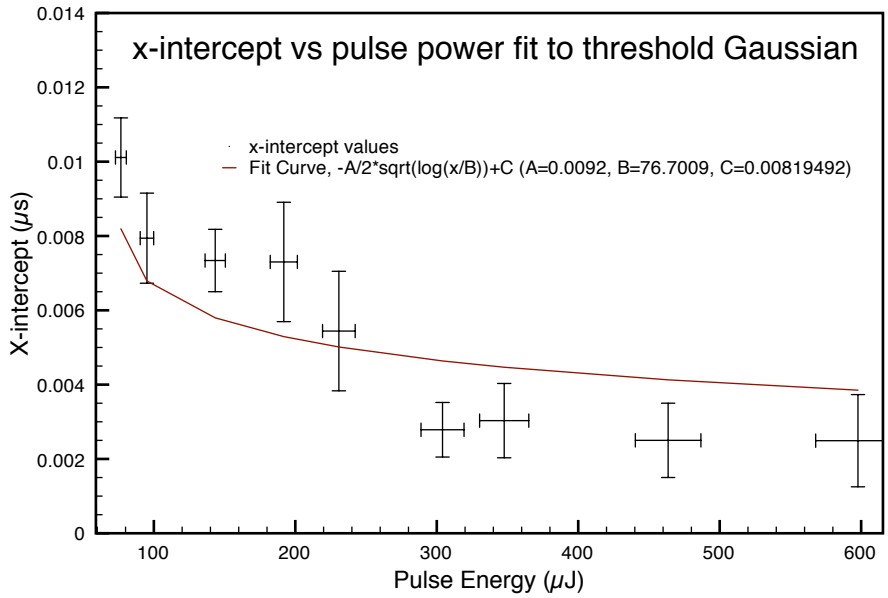

Fig. 6. Shock wave positions' x-intercept vs pulse power as found in Fig. 5 fit to equation 3

the trend in the plot points to a ratio of zero that occurs around $55\mu J/pulse$. This low energy transfer found agrees well with transmission measurements where there was no observable change in laser energy for per pulse energies from 1 to $100\mu J$.

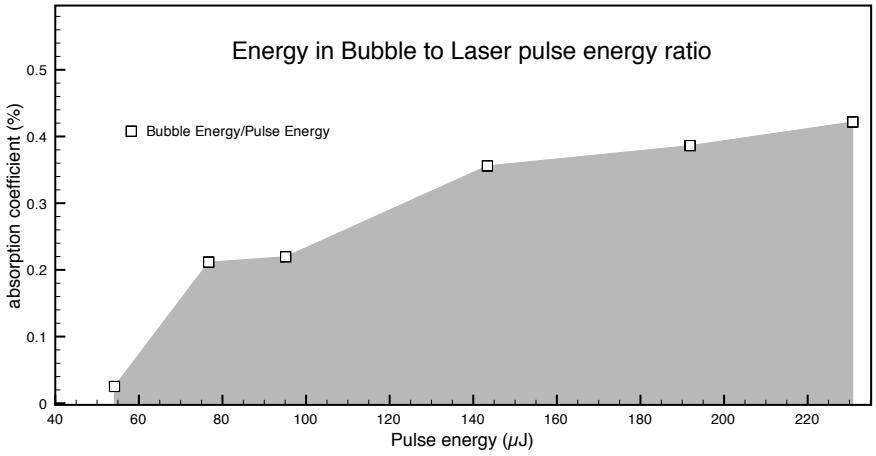

Fig. 7. Ratio of energy in the bubble to energy in the laser pulse. Bubble energy was inferred from equation 4

4. Conclusion

We used of a pair of Nd:YAG lasers, where the pump laser is frequency doubled and the probe laser was used in the fundamental $1.064\mu m$. Timing delays were synchronized to a CCD and controlled by a DG535 delay generator. We show the life cycle of a laser generated bubble in agar gel. The formation of the bubble is marked first by the generation of a shock wave, and then the growth, collapse and formation of quazi-stable bubble which lasted for more then a second. The shock wave was generated before the 9ns laser pulse had finished. The maximum and farfield bubble sizes were shown to be linearly related. Using equation 4 the energy in the bubble was inferred and an approximate threshold of bubble formation of $55\mu J/pulse$ was given, in accordance with observations. Using a simplified model to associate the shock wave generation time with an irradiance threshold gave an energy threshold of $74\mu J/pulse$. When the energy in the bubble to energy in the laser pulse ration was considered, an increased absorption of laser power is seen, which can be accounted for by the onset of plasma in the focal region. This seems to agree well with other authors on the subject, that bubble formation is the after effect of a laser generated plasma. While Rau gives observational evidence of the plasma formation by looking for a spark with the lab lights off, a proper analysis of the laser produced plasma would offer insight to the event. What is clear, is that the process is inherently nonlinear, and not stress confined.